Two-dimensional visible synchrotron light interferometry for transverse beam-profile measurement at the SPring-8 storage ring

Mitsuhiro Masaki* and Shiro Takano

Japan Synchrotron Radiation Research Institute, SPring-8, Mikazuki, Hyogo 679-5198, Japan.
E-mail: masaki@spring8.or.jp

A two-dimensional visible synchrotron light interferometer has been developed to measure the transverse profile of an electron beam at the SPring-8 storage ring. The new interferometer enables the simultaneous measurement of beam sizes along the major and minor axes and the beam-tilt angle of an assumed elliptical Gaussian distribution. The principle of the interferometer is explained through basic formulae. To calibrate the point-spread function of the interferometer, a simple error model was assumed for disturbances in the amplitude and phase of the light; these disturbances were presumably caused by optical elements, such as mirrors and lenses. The experimental method to determine the parameters in the error model is shown. To verify the two-dimensional profiling capabilities of the interferometer, an electron beam stored in the SPring-8 storage ring operated at various working points was observed. A beam broadening from 20 to 120 μm in the vertical direction and changes in the beam-tilt angle were clearly observed at working points close to the differential resonance. However, the vertical spatial resolution is limited by the available vertical separation of the apertures of the diffracting mask because of the narrow aperture of the upstream vacuum duct.

Keywords: two-dimensional interferometry; point-spread function; beam size; beam tilt; emittance.

1. Introduction

The emittance of an electron beam, which is inversely proportional to the brilliance of the synchrotron radiation, is one of the most important characteristics of a storage ring operated as a synchrotron light source. To monitor degradation of the emittance, which could be caused by beam instabilities or ion-trapping phenomena, it is necessary to observe the transverse profile of the electron beam in real time. Therefore, a non-destructive beam-profile monitor is indispensable for the operation of light-source accelerators. Conventionally, the imaging of an electron beam (*e.g.* Hoffmann & Meot, 1982) using visible synchrotron light has been applied to non-destructive beam-profile measurements.

Third-generation synchrotron light sources such as the SPring-8 storage ring are designed to achieve low emittance and a small emittance-coupling ratio. The vertical beam size of such a light source is no larger than the diffraction-limited resolution of the imaging method using visible synchrotron radiation. Interferometry is an alternative method for object-size measurement that overcomes the diffraction-limited resolution (Fizeau, 1868; Michelson, 1920). The diffraction-limited resolution of an imaging system can be defined as the r.m.s. width, $\sigma_{\rm image}$, of the main peak of the point-spread function (*i.e.* of the image of a point source emitting coherent light). In the case of an interferometer, we can similarly define the 'resolution' for size measurement as the r.m.s. width, $\sigma_{\rm inter}$, of each fringe of the 'point-spread function' (*i.e.* the interference pattern of a point source emitting coherent light). If the imaging system and the interferometer have the same observing wavelength and the same acceptance angle, the width, $\sigma_{\rm inter}$, of the point-spread function of the interferometer is about half of the width, $\sigma_{\rm image}$, of the imaging system. In other words, the resolution of the interferometer is two times better for object-size measurements than the imaging method.

Visible light interferometry has been applied to beam-size measurements of electron storage rings in the past. For example, the transverse beam size of the Siberia-1 450 MeV electron storage ring was measured by interferometers using Lloyd's mirrors (Chubar, 1995). Interferometers using a classical Young's double slit were applied to beam-size measurements at the Photon Factory storage ring of KEK (Mitsuhashi, 1997). A small vertical beam size (1σ) of 14.8 μm was successfully measured by an interferometer using a double slit at the damping ring of ATF of KEK (Mitsuhashi & Naito, 1998), and the superior resolution of interferometry for beam-size measurement was demonstrated. We have also employed Young's double slits in order to measure the vertical beam size at the SPring-8 storage ring (Masaki *et al.*, 1999). Another advantage of interferometry using a classical double slit over the imaging method is that the mirror used to separate the visible light component of the synchrotron radiation can be free from thermal deformation, as it is not necessary to expose the mirror to synchrotron radiation on the electron orbit plane, where most of the power of the synchrotron radiation is localized.

A disadvantage of interferometers using a classical double slit, however, is that the available information about the beam profile is essentially one-dimensional at any given time. Simultaneous two-dimensional information about the transverse beam profile is lost, and only the beam size projected in one direction, which is determined by the configuration of the double slit, is obtained. We have developed a novel visible synchrotron light interferometer that enables us to obtain two-dimensional information about the transverse profile of an electron beam at a point in time. This interferometer exhibits a superior resolution, similar to interferometers using a classical double slit. The new interferometer uses a diffracting mask with four apertures distributed at the corners of a rectangle. A two-dimensional interference pattern results from the superposition of the four partially coherent light beams that pass through the apertures. This interference pattern includes information on beam sizes as projected in the horizontal, vertical and two diagonal directions. The electron beam in radiation equilibrium closely approximates a Gaussian distribution. Therefore, the transverse beam profile is characterized by three parameters: the beam sizes along the major and the minor axes, and the tilting angle of the major axis. These three parameters are determined by fitting a model function, which is obtained by convoluting the point-spread function with an elliptical Gaussian distribution, to the observed two-dimensional interference pattern.

In this paper, we explain the principle of two-dimensional interferometry in §2. We describe the two-dimensional interferometer installed in the SPring-8 storage ring in §3, the experimental method to calibrate the point-spread function of the interferometer in §4, and the results of the beam-profile measurement in §5.

2. Principle of two-dimensional interferometry

2.1. Point-spread function

The two-dimensional interferometer uses synchrotron radiation emitted from an electron beam moving in a field of a bending magnet in a storage ring. In the interferometer, monochromatic light is selected from the bending-magnet radiation by a band-pass filter. The

monochromatic light from a single electron is not a spherical wave in a strict sense. However, it is important that the monochromatic light approximates to a spherical wave, since the interferometer is based on the van Citter–Zernike theorem (*e.g.* Born & Wolf, 1980), which relates the spatial coherence of incoherent light from stationary point sources to the source size. The required conditions for spherical-wave approximation are described in Appendix *A*. The interferometer described in §3 satisfies the conditions sufficiently. In the discussions below, we assume that radiation from a single electron is a spherical wave emitted at a source point in a bending magnet.

A diffracting mask with four circular apertures is placed at a distance L_0 from a source point, as shown in Fig. 1. Each aperture of the mask is centered at a corner of a rectangle; the positions of the apertures are (X_n, Y_n) (n = 1, 2, 3 and 4) and the diameter of each aperture is d. On the diffracting mask, the electric field of the monochromatic light emitted by a single electron is expressed as

$$E_s(x_s, y_s; x_e, y_e) = A_0 \exp(-2\pi i R_0/\lambda)/R_0, \quad (1)$$

where λ is the wavelength, R_0 is the distance between the position (x_e, y_e) of a single electron and the point (x_s, y_s) on the mask, and A_0 is the amplitude. The light diffracted by the mask is focused on an observation screen at a distance L_s from the mask by a lens with focal length F. The electric field on the screen is calculated *via* the Reyleigh–Sommerfeld diffraction formula,

$$E(x, y; x_e, y_e) = (i/\lambda) \int_s \{L_s R_s^{-2} E_s(x_s, y_s; x_e, y_e) \times \exp[2\pi i (x_s^2 + y_s^2)/2F\lambda] \exp(-2\pi i R_s/\lambda)\, dx_s\, dy_s\}, \quad (2)$$

where the integral is evaluated on each aperture of the mask. R_s is the distance between a point (x_s, y_s) on the mask and a point (x, y) on the observation screen. Using a paraxial approximation, the electric field on the observation screen is further reduced to

$$E(x, y; x_e, y_e) = \pi A_0 d^2 (2\lambda L_s L_0)^{-1} \exp(-iP)\,[J_1(R)/R] \times \sum_{n=1}^{4} \exp\{(2\pi i/\lambda)[(x_e/L_0 + x/L_s)X_n + (y_e/L_0 + y/L_s)Y_n]\}, \quad (3)$$

where $J_1(R)$ denotes the first-order Bessel function, and

$$R = (\pi d/\lambda)[(x_e/L_0 + x/L_s)^2 + (y_e/L_0 + y/L_s)^2]^{1/2}. \quad (4)$$

The phase function P is not observable and is not important here. If we define the positions of the centers of each aperture of the mask as $(X_1, Y_1) = (D_x/2, D_y/2)$, $(X_2, Y_2) = (-D_x/2, D_y/2)$, $(X_3, Y_3) = (-D_x/2, -D_y/2)$ and $(X_4, Y_4) = (D_x/2, -D_y/2)$, the light intensity on the screen is given by

$$\begin{aligned} I(x, y; x_e, y_e) &= |E(x, y; x_e, y_e)|^2 \\ &= \{\pi A_0 d^2 (2\lambda L_s L_0)^{-1} [J_1(R)/R]\}^2 \\ &\quad \times \{1 + \cos[(2\pi/\lambda)(x_e/L_0 + x/L_s)D_x]\} \\ &\quad \times \{1 + \cos[(2\pi/\lambda)(y_e/L_0 + y/L_s)D_y]\}. \end{aligned} \quad (5)$$

Equation (5), which describes the two-dimensional interference pattern formed by diffraction of the monochromatic light from a single electron, is the point-spread function of the interferometer.

2.2. Effect of electron-beam distribution

The normalized transverse distribution of electrons, ρ, on the $x_e y_e$ plane including a source point in Fig. 1 is assumed to be an elliptical Gaussian distribution, centered at a position (x_0, y_0) and having a tilt angle of θ,

$$\rho(x_e, y_e) = (2\pi\sigma_I\sigma_{II})^{-1} \exp\{-[a(x_e - x_0)^2 + b(y_e - y_0)^2 + c(x_e - x_0)(y_e - y_0)]/2\}. \quad (6)$$

The parameters a, b and c are given by

$$a = (\cos\theta/\sigma_I)^2 + (\sin\theta/\sigma_{II})^2, \quad (7)$$

$$b = (\sin\theta/\sigma_I)^2 + (\cos\theta/\sigma_{II})^2, \quad (8)$$

$$c = (\sigma_I^{-2} - \sigma_{II}^{-2}) \sin 2\theta, \quad (9)$$

where σ_I and σ_{II} are the beam sizes along the major and minor axes, respectively. An observed interference pattern is a convolution of the point-spread function, (5), with the distribution of electrons, (6), and can be expressed by the following function,

$$\begin{aligned} \tilde{I}(x, y) &= \int_{-\infty}^{\infty} I(x, y; x_e, y_e)\, \rho(x_e, y_e)\, dx_e dy_e \\ &= \left(\frac{\pi A_0 d^2}{2\lambda L_s L_0} \frac{J_1\{(\pi d/\lambda)[(x/L_s + x_0/L_0)^2 + (y/L_s + y_0/L_0)^2]^{1/2}\}}{(\pi d/\lambda)[(x/L_s + x_0/L_0)^2 + (y/L_s + y_0/L_0)^2]^{1/2}}\right)^2 \\ &\quad \times (1 + \text{interference terms}), \end{aligned} \quad (10)$$

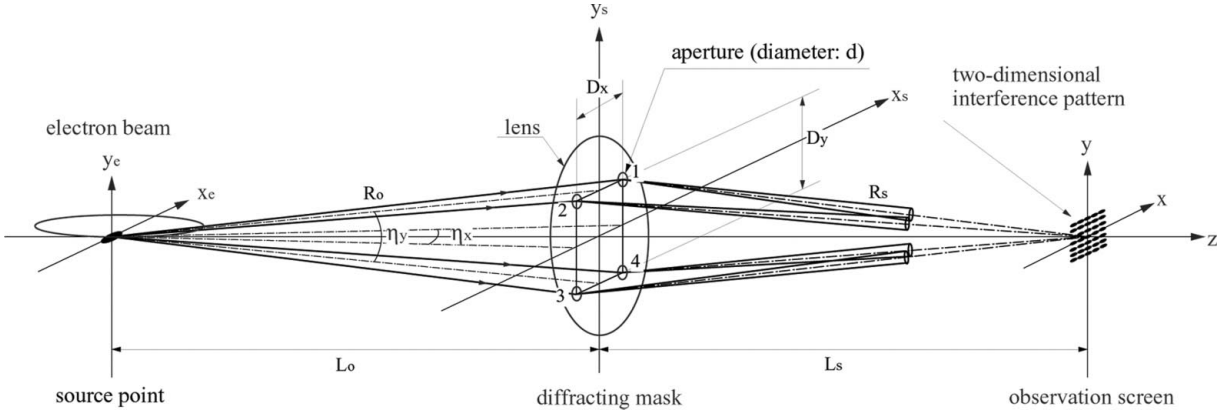

Figure 1
Principle of a two-dimensional synchrotron light interferometer. An electron is assumed to emit a spherical wave at the source point in a bending magnet. The wavefront is divided by four apertures of a diffracting mask. Divided light waves are superposed by lenses to form two-dimensional interference fringes on the observation screen.

where the interference terms are

$$V_{12}\cos\left[\frac{2\pi D_x}{\lambda}\left(\frac{x}{L_s}+\frac{x_0}{L_0}\right)\right]+V_{14}\cos\left[\frac{2\pi D_y}{\lambda}\left(\frac{y}{L_s}+\frac{y_0}{L_0}\right)\right]$$
$$+\frac{1}{2}V_{13}\cos\left\{\frac{2\pi}{\lambda}\left[D_x\left(\frac{x}{L_s}+\frac{x_0}{L_0}\right)+D_y\left(\frac{y}{L_s}+\frac{y_0}{L_0}\right)\right]\right\}$$
$$+\frac{1}{2}V_{24}\cos\left\{\frac{2\pi}{\lambda}\left[D_x\left(\frac{x}{L_s}+\frac{x_0}{L_0}\right)-D_y\left(\frac{y}{L_s}+\frac{y_0}{L_0}\right)\right]\right\}. \quad (11)$$

The convolution integral of the envelope part, $[J_1(R)/R]^2$, was neglected above, by assuming that the width of the envelope is much larger than the beam size, namely,

$$2\pi^2 d(\sigma_{\rm I}+\sigma_{\rm II})/\lambda L_0 \ll 1. \quad (12)$$

The interference term expressed by (11) results from the superposition of the four partially coherent light beams that pass though the four apertures of the diffracting mask. The factors V_{nm} ($n, m = 1$, 2, 3 and 4) are referred to as visibilities and represent the degree of spatial coherence between the nth and the mth apertures on the diffracting mask in Fig. 1. The visibility factors V_{nm} are expressed by

$$V_{nm}=\exp\left[-2(\pi\sigma_{nm}\eta_{nm}/\lambda)^2\right], \quad n, m = 1, 2, 3, 4. \quad (13)$$

The parameters η_{nm} are the angular separations of the four apertures, with $\eta_{12} = D_x/L_0$, $\eta_{14} = D_y/L_0$ and $\eta_{13} = \eta_{24} = (D_x^2 + D_y^2)^{1/2}/L_0$. The parameters σ_{nm} are the electron beam sizes projected in the horizontal, vertical and two diagonal directions determined by the configuration of the diffracting mask. These paramters are given by

$$\sigma_{12} = \sigma_{34} = (\sigma_{\rm I}^2\cos^2\theta + \sigma_{\rm II}^2\sin^2\theta)^{1/2}, \quad (14)$$

$$\sigma_{14} = \sigma_{23} = (\sigma_{\rm I}^2\sin^2\theta + \sigma_{\rm II}^2\cos^2\theta)^{1/2}, \quad (15)$$

$$\sigma_{13} = \left[\sigma_{\rm I}^2\cos^2(\theta-\Theta) + \sigma_{\rm II}^2\sin^2(\theta-\Theta)\right]^{1/2}, \quad (16)$$

$$\sigma_{24} = \left[\sigma_{\rm I}^2\cos^2(\theta+\Theta) + \sigma_{\rm II}^2\sin^2(\theta+\Theta)\right]^{1/2}, \quad (17)$$

where $\Theta = \cos^{-1}[D_x/(D_x^2 + D_y^2)^{1/2}]$ is the angle between the horizontal direction and the diagonal line connecting apertures 1 and 3. The sizes $\sigma_{\rm I}$ and $\sigma_{\rm II}$ and the tilt angle, θ, of the electron beam are determined by fitting the model function expressed by (10) to the observed two-dimensional interference pattern.

3. Experimental setup of the two-dimensional interferometer of the SPring-8 storage ring

The experimental setup of the two-dimensional interferometer of the SPring-8 storage ring is shown in Fig. 2. All the instruments were temporally installed in the space in the accelerator tunnel, of the front end of beamline BL14B2, that is reserved for future installations. The visible light emitted from the point source in the bending magnet is steered towards the interferometer by two plane mirrors. The first mirror, which is in a vacuum chamber, consists of an oxygen-free copper base with an aluminium coating, protected by a membrane of SiO_2. The flatness of this mirror is $\lambda/5$ (λ = 632.8 nm). The second mirror, which is exposed to the atmosphere, consists of a Pyrex glass base with an aluminium coating, protected by a membrane of MgF_2. The flatness of this mirror is $\lambda/10$. Neither mirror is water-cooled. A water-cooled photon absorber made of oxygen-free copper (horizontal and vertical dimensions of 70 and 16 mm, respectively) is placed in front of the first mirror to protect it from the heat load of the synchrotron radiation. The light passes through the upper and lower apertures (horizontal by vertical size = 70 × 22 mm) of the photon absorber. A view window (diameter 4″ and thickness 0.5″), made of a fused silica glass with $\lambda/8$ flatness, is sandwiched between two flanges, with a groove for a helicoflex vacuum seal to preserve the original flatness of the glass.

A diffracting mask with four circular apertures (3 mm diameter) centered at the corners of a 13 × 30 mm rectangle is placed 19.6 m from the source point. The accuracy of the position and diameter of each circular aperture of the mask is a few micrometers, and the horizontal and vertical angular separations, η_{12} and η_{14}, of the apertures viewed from the source point are 0.662 and 1.53 mrad, respectively. To calibrate the interferometer by the method detailed in §4, a movable screen is placed in front of the diffracting mask, thus allowing each aperture to be closed independently.

The optimum separations of the four apertures of the mask depend on the target size to be measured and the observing wavelength. If the separation is too large, the interference fringes disappear and it is hardly possible to distinguish valleys and peaks in the interference pattern. On the other hand, if the separation is too small, the visibility approaches unity and it is hardly possible to distinguish the intensity of valleys in the interference pattern from the intensity of the background. The optimal condition of an interference pattern for size measurement is that the valleys have half the intensity of the peaks,

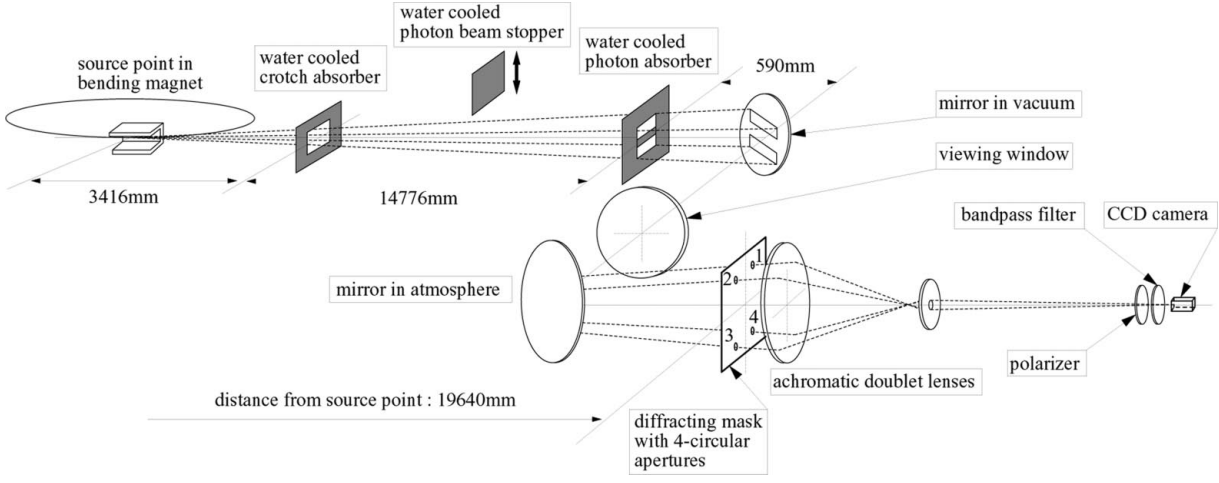

Figure 2
Schematic view of the experimental setup of the two-dimensional interferometer at the SPring-8 storage ring.

which gives a visibility of 1/3. This visibility is attainable when the r.m.s. width, $\sigma_{\rm inter}$, of the point-spread function of the interferometer (defined in §1) is about 0.8 times the 1σ beam size. The horizontal separation, η_{12}, of the SPring-8 interferometer has been optimized for the designed value of the horizontal beam size at the point source. On the other hand, the vertical separation, η_{14}, has not been optimized, because the upstream vacuum duct limits the available aperture to 2.2 mrad. The upstream vacuum duct itself has been designed to transport X-rays to beamline BL14B2 for users' experiments and is not optimized for transporting visible synchrotron light, which has a larger vertical divergence than X-rays. The widths $\sigma_{\rm inter}$ of the point-spread function of the SPring-8 interferometer are 121 and 52 μm in the horizontal and vertical directions, respectively.

Light passing through each aperture is focused on a CCD camera (pixel size = 7.6 × 7.6 μm), equipped with an electric shutter, by two achromatic doublet lenses. The second lens and the CCD camera are axially movable, so that magnification is adjustable to about unity. The electric shutter is useful for avoiding resolution degradation caused by mechanical vibrations of the optical components. The exposure time was 4.82 ms in the experiment described in §5. In front of the CCD camera, we placed a polarizer (extinction ratio = 5×10^{-4}), in order to select only the σ-polarized component of light, and a bandpass filter (center wavelength = 443.38 nm, FWHM = 10 nm), in order to obtain quasi-monochromatic light.

Observed interference patterns are saved on a PC with an image capture board. Background data are measured by closing the photon beam stopper shown in Fig. 2, which can shield all the light passing through the aperture of the upstream crotch absorber. To obtain a linearity curve of the CCD camera (*i.e.* the output intensity as a function of the incident light intensity), we measured the peak intensity of the diffraction pattern obtained with a single aperture of the mask opened as a function of the beam current of the storage ring.

The narrow vacuum duct described above causes a problem with stray light, which results from reflections of visible synchrotron radiation on the inner surface of the vacuum duct. Removing the diffracting mask and moving the second lens axially, we observed multiple spots as evidence of the existence of this stray light.

4. Calibration of the interferometer

4.1. Error model of the amplitude and the phase of light

In a real interferometer, the amplitude and phase distributions of the light incident on the observation screen are different from the ideal distributions because of distortion by optical elements and by contamination of the stray light mentioned in §3. It is difficult to formulate and evaluate the effects of stray light on the amplitude and phase distributions of the incident light. Therefore, we do not take account of the effect of stray light when we formulate an error model for the amplitude and phase below. The effect of stray light will be discussed in §5, where we describe the results of our beam-size measurement. The disturbance in amplitude may result from the uneven reflectivity or transmissivity of optical elements, such as the view window, mirrors, lenses and polarizer. The error in the phase may result from distortions of reflected and transmitted wavefronts by the optical elements. The disturbances in amplitude and phase distort the ideal point-spread function expressed by (5), and the effect of this distortion appears as the local degradation of the visibility of the point-spread function. In order to calibrate the interferometer, it is necessary to investigate the effects of these disturbances by an experimental method and to modify the ideal point-spread function.

For mathematical simplicity, we assume a model in which amplitude and phase errors are defined on the diffracting mask. Propagating the light emitted from a point source and passing through the nth aperture of the diffracting mask, we can express the electric field on the observation screen (CCD camera) as

$$\begin{aligned} E_n(x, y; x_{\rm e} y_{\rm e}) = i(\lambda L_s L_0)^{-1} \exp(-iP) \int\limits_{S_n} \big(B_n(x_s, y_s) \exp\big\{(2\pi i/\lambda) \\ \times \big[(x_{\rm e}/L_0 + x/L_s)\, x_s + (y_{\rm e}/L_0 + y/L_s)\, y_s\big] \\ + i\Phi_n(x_s, y_s)\big\}\big)\, {\rm d}x_s\, {\rm d}y_s, \end{aligned} \tag{18}$$

where the real functions $B_n(x_s, y_s)$ and $\Phi_n(x_s, y_s)$ describe the amplitude of the electric field and the phase error, respectively, on the nth aperture of the diffracting mask. The phase error, Φ_n, can be expanded as a polynomial of the deviation, (X_n, Y_n), from the center of each aperture as

$$\Phi_n(x_s, y_s) = \varphi_n + \xi_n(x_s - X_n) + \zeta_n(y_s - Y_n) + \text{higher orders}. \tag{19}$$

If we temporally set the amplitude $B_n(x_s, y_s)$ to a constant value, C_n, and consider the terms of (19) up to the first order, the integral in (18) can be analytically executed as follows,

$$\begin{aligned} E_n(x, y;\, x_{\rm e}, y_{\rm e}) = iA_n \exp(-iP)\big[J_1(R_n)/R_n\big] \exp\big\{(2\pi i/\lambda) \\ \times \big[(x_{\rm e}/L_0 + x/L_s)\, X_n + (y_{\rm e}/L_0 + y/L_s) Y_n\big] + i\varphi_n\big\}, \end{aligned} \tag{20}$$

where

$$R_n = (\pi d/\lambda)\Big\{\big[x_{\rm e}/L_0 + (x - x_n)/L_s\big]^2 + \big[y_{\rm e}/L_0 + (y - y_n)/L_s\big]^2\Big\}^{1/2}, \tag{21}$$

and $(x_n, y_n) = (-\lambda L_s \xi_n/2\pi,\ -\lambda L_s \zeta_n/2\pi)$. The coefficient $\pi C_n d^2/(2\lambda L_s L_0)$ is replaced by a parameter A_n. The position dependence of the amplitude $B_n(x_s, y_s)$ and the higher-order terms of the phase error influence the shape of the envelope $J_1(R_n)/R_n$ of the electric field. To consider such effects, we replace R_n by

$$\begin{aligned} R_n = (\pi d/\lambda)\Big\{\alpha_n\big[x_{\rm e}/L_0 + (x - x_n)/L_s\big]^2 + \beta_n\big[y_{\rm e}/L_0 + (y - y_n)/L_s\big]^2 \\ + \gamma_n\big[x_{\rm e}/L_0 + (x - x_n)/L_s\big]\big[y_{\rm e}/L_0 + (y - y_n)/L_s\big]\Big\}^{1/2}. \end{aligned} \tag{22}$$

To calibrate the point-spread function of the interferometer, it is necessary to determine experimentally the parameters A_n, α_n, β_n, γ_n, φ_n, ξ_n and ζ_n. It is also necessary to obtain experimentally the effective value of L_s, which relates to the pitch of the interference fringes, because the error model assumes one lens, while the optical system of the SPring-8 interferometer incorporates two lenses.

4.2. Experimental methods to determine the error parameters

The parameters A_n, α_n, β_n, γ_n, x_n and y_n (n = 1, 2, 3 and 4), which are related to the envelope of the electric field, (20), can be determined by observing an intensity distribution with the nth aperture of the diffracting mask opened while the other apertures are closed. If we assume that the position of the electron beam is at the origin, $(x_0, y_0) = (0, 0)$, on the source plane, the intensity distribution on the screen is given by the model function $H_n(x, y)$,

$$\begin{aligned} H_n(x, y) &= \int\limits_{-\infty}^{\infty}\int |E_n(x, y; x_{\rm e}, y_{\rm e})|^2\, \rho(x_{\rm e}, y_{\rm e})\, W(\lambda)\, {\rm d}x_{\rm e}\, {\rm d}y_{\rm e}\, {\rm d}\lambda \\ &\simeq |E_n(x, y; 0, 0)|^2 \\ &= A_n^2\big[J_1(Z_n)/Z_n\big]^2, \end{aligned} \tag{23}$$

$$Z_n = \frac{\pi d}{\lambda}\left[\alpha_n\left(\frac{x-x_n}{L_s}\right)^2+\beta_n\left(\frac{y-y_n}{L_s}\right)^2+\gamma_n\left(\frac{x-x_n}{L_s}\right)\left(\frac{y-y_n}{L_s}\right)\right]^{1/2}, \quad n = 1, 2, 3, 4. \tag{24}$$

If the diameter, d, of each aperture is sufficiently small, the width of the envelope of the observed intensity distribution is much larger than the beam size, and the effect of the electron distribution, ρ, given by (6) is negligible. The effect of convolution with the wavelength spectrum, $W(\lambda)$, of the bandpass filter can be included in the parameters α_n, β_n and γ_n, which express the shape of the envelope. Parameters A_n, α_n, β_n, γ_n, x_n and y_n can be determined by fitting the function $H_n(x, y)$ to the observed intensity distribution. The first-order phase errors, ξ_n and ζ_n, can be obtained from x_n and y_n, respectively.

We can determine the parameter L_s and the phase offset φ_n by observing the interference pattern with two apertures, *viz.* the nth and the mth, opened. The parameter L_s is obtained from the pitch of the interference fringes and the relative position of the two apertures. The difference in the phase offset, $\varphi_n - \varphi_m$, is obtained from the phase of the interference fringes with respect to the envelope peak of the interference pattern. The interference pattern is described by the function $G_{nm}(x, y)$,

$$\begin{aligned} G_{nm}(x, y) &= \int_{-\infty}^{\infty}\int \left[|E_n(x, y; x_e, y_e) + E_m(x, y; x_e, y_e)|^2 \right. \\ &\quad \left. \times \rho(x_e, y_e)\, W(\lambda)\right] \mathrm{d}x_e\, \mathrm{d}y_e\, \mathrm{d}\lambda \\ &= H_n(x, y) + H_m(x, y) + Q_{nm}(x, y). \end{aligned} \tag{25}$$

The term $Q_{nm}(x, y)$ is an interference term,

$$\begin{aligned} Q_{nm}(x, y) = 2\big[H_n(x, y)\, H_m(x, y)\big]^{1/2} \int_{-\infty}^{\infty} \big\{W(\lambda) \exp\big[-2(\pi\sigma_{nm}\eta_{nm}/\lambda)^2\big] \\ \times \cos\big[(2\pi/\lambda)(p_{nm}x + q_{nm}y) + \varphi_{nm}\big]\big\}\, \mathrm{d}\lambda, \end{aligned} \tag{26}$$

where the parameters p_{nm} and q_{nm}, which include information about L_s, are defined as

$$p_{nm} = \big[(X_n - X_m)\cos\varphi + (Y_n - Y_m)\sin\varphi\big]/L_s, \tag{27}$$

$$q_{nm} = \big[-(X_n - X_m)\sin\varphi + (Y_n - Y_m)\cos\varphi\big]/L_s. \tag{28}$$

The parameter φ_{nm} represents $\varphi_n - \varphi_m$, and φ is the tilt of the CCD camera relative to the diffracting mask. The functions H_n and H_m denote the envelope given by (23), with A_n, α_n, β_n, γ_n, x_n and y_n (n = 1, 2, 3 and 4) determined above. The parameters p_{nm}, q_{nm} and φ_{nm}, which relate to the horizontal and vertical pitches and the phase offset of the interference fringes, respectively, can be determined by fitting the model function $G_{nm}(x, y)$ to the observed interference patterns. There are six combinations that involve two out of the four apertures. The free parameter σ_{nm} expresses a beam size projected onto a line connecting the nth and mth apertures. Fig. 3 shows examples of the interference patterns observed by opening two apertures of the diffracting mask.

4.3. Modified point-spread function

The modified point-spread function of the two-dimensional interferometer can be expressed by the following formula, which includes the error parameters,

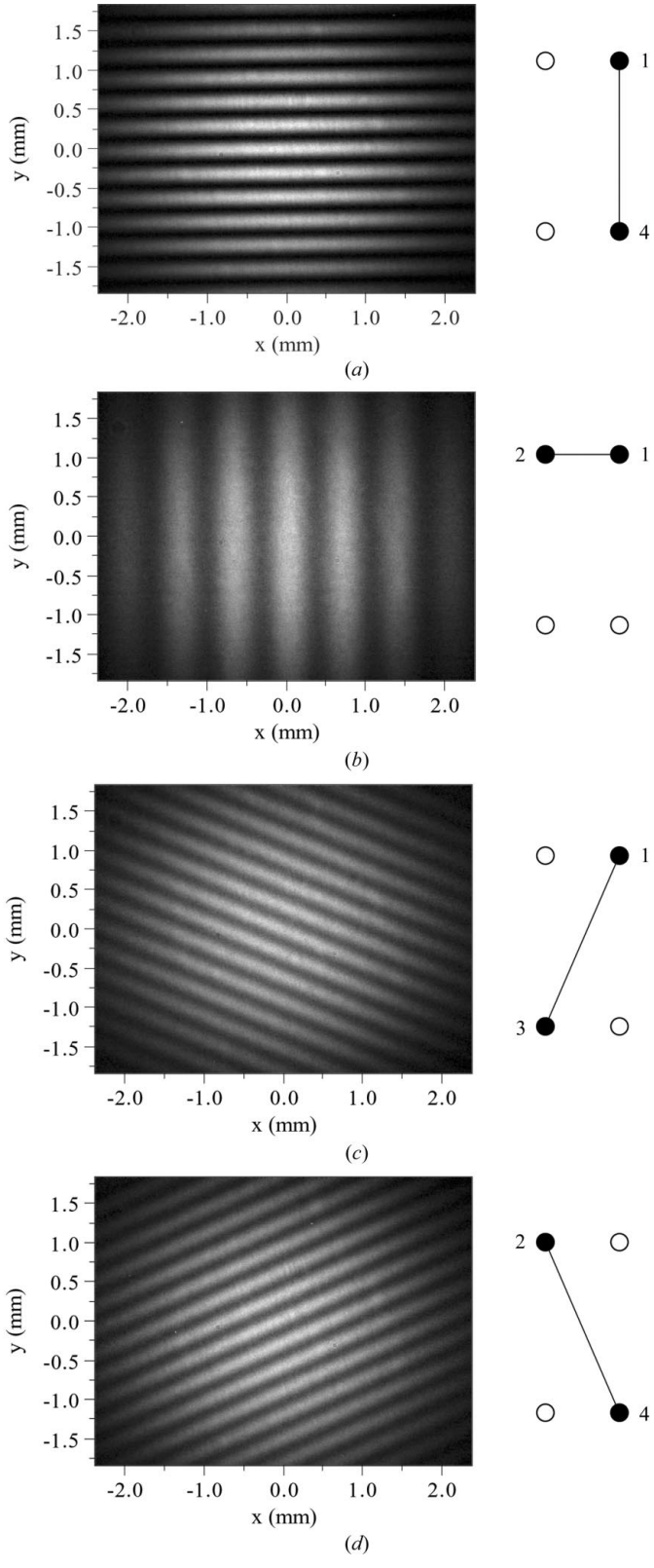

Figure 3
Interference patterns observed when two out of the four apertures of the diffracting mask were opened while the others remained closed. (*a*) The interference pattern for a vertical pair of apertures (numbers 1 and 4 of Fig. 2). (*b*) The pattern for a horizontal pair of apertures (1 and 2). (*c*) The pattern for a diagonal pair of apertures (1 and 3). (*d*) The pattern for the other diagonal pair of apertures (2 and 4).

$$I(x, y; x_e, y_e) = \int_{-\infty}^{\infty} W(\lambda)\left|\sum_{n=1}^{4} E_n(x, y; x_e, y_e)\right|^2 d\lambda$$
$$= \sum_{n=1}^{4} H_n(x, y) + 2\sum_{n>m}\left[H_n(x, y)\, H_m(x, y)\right]^{1/2}$$
$$\times \int_{-\infty}^{\infty}\left\{W(\lambda)\cos\left[(2\pi/\lambda)\left(p_{nm}x + q_{nm}y + \frac{X_n - X_m}{L_0}x_e + \frac{Y_n - Y_m}{L_0}y_e\right) + \varphi_{nm}\right]\right\} d\lambda. \quad (29)$$

For the two-dimensional interferometer of the SPring-8 storage ring, the error parameters A_n, α_n, β_n, γ_n, x_n, y_n, p_{nm}, q_{nm} and φ_{nm} were experimentally determined *via* the method described above. The point-spread function, (29), with the determined error parameters, is shown in Fig. 4, in which the position of a single electron is assumed to be at the origin, $(x_e, y_e) = (0, 0)$, on the source plane.

We can obtain parameters σ_I, σ_{II} and θ, which characterize the transverse beam profile, by fitting the following model function to the observed two-dimensional interference pattern,

$$\tilde{I}(x, y) = N_0 \int_{-\infty}^{\infty} I(x - x_c, y - y_c; x_e, y_e)\, \rho(x_e, y_e)\, dx_e\, dy_e$$
$$= N_0\left[\sum_{n=1}^{4} H_n(x - x_c, y - y_c) + \sum_{n>m} Q_{nm}(x - x_c, y - y_c)\right]. \quad (30)$$

Equation (30) is the modified point-spread function, (29), convoluted with the distribution of electrons, ρ.

5. Beam-profile measurements of the SPring-8 storage ring

5.1. Beam size and tilt angle

The transverse beam profile of the SPring-8 storage ring was observed with the two-dimensional synchrotron light interferometer. To examine the capability of the interferometer for two-dimensional profiling, the storage ring was operated at various working points. The horizontal betatron tune, ν_x, was varied from 40.15 to 40.60 across the differential resonance condition, while the vertical betatron tune, ν_y, was fixed at 18.35. The filling pattern of the stored beam was 21 equally spaced bunches at 1 mA bunch^{-1}, which results in a total beam current of 21 mA. The magnet gaps of all the insertion devices were fully opened in order to minimize the effects of the insertion devices on the beam emittance.

Examples of observed two-dimensional interference patterns are shown in Fig. 5. Fig. 5(*a*) shows an interference pattern at a working point $(\nu_x, \nu_y) = (40.15, 18.35)$, which is close to the condition for users' time operation, while Figs. 5(*b*) and 5(*c*) show patterns at working points near the differential resonance, $(\nu_x, \nu_y) = (40.35, 18.35)$. In Fig. 6, the measured beam sizes, σ_I and σ_{II}, and the beam tilt angle, θ, are plotted as functions of the horizontal tune. Error bars denote the statistical error (1σ) calculated from fluctuations of the values measured five times at each working point. The beam size σ_{II} increases near the differential resonance, showing an increase of the emittance-coupling ratio at the differential resonance. The change in θ near the differential resonance is evident. Changes in

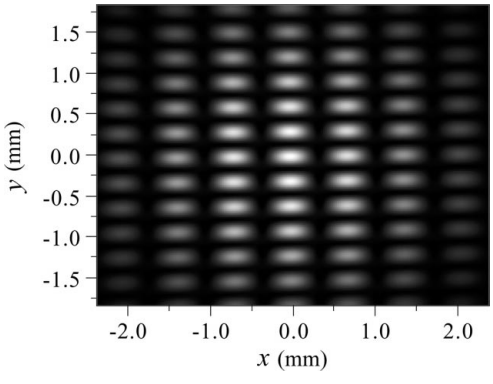

Figure 4
The point-spread function of the two-dimensional interferometer at the SPring-8 storage ring. The point-spread function was calibrated by the procedures described in the text.

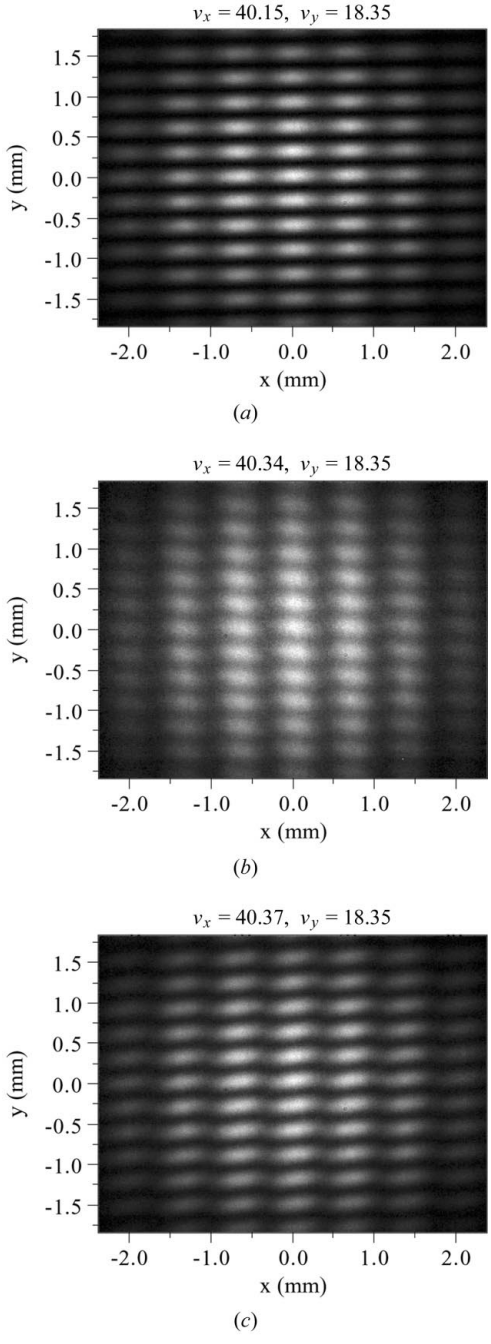

Figure 5
Examples of observed two-dimensional interference patterns. The interference patterns at (*a*) the working point close to the condition for users' time operation, and (*b*) and (*c*) the working points near the differential resonance line $(\nu_x, \nu_y) = (40.35, 18.35)$.

$\sigma_{\rm I}$, $\sigma_{\rm II}$ and θ were also clearly observed near the sum resonance, $(\nu_x, \nu_y) = (40.65, 18.35)$.

The measured horizontal beam size was $\sigma_x \simeq \sigma_{\rm I} = 150.0 \pm 0.1$ µm at the working point $(\nu_x, \nu_y) = (40.15, 18.35)$ close to the user's time operation. We neglected the small tilt angle of the beam. The resolution or the width, $\sigma_{\rm inter}$, of the point-spread function of the interferometer is 121 µm in the horizontal direction, which is optimal for a horizontal beam size of 150 µm and gives a corresponding visibility of about 1/3. Therefore, we consider that the measured horizontal beam size is reliable. On the other hand, the vertical beam size measured at the same working point was $\sigma_y \simeq \sigma_{\rm II} = 21.8$ µm. The vertical beam size is smaller than the vertical width, $\sigma_{\rm inter}$, of the point-spread function (52 µm, as described in §3). Thus, the resolution of the interferometer is not sufficient to measure the vertical beam size. In this situation, the accuracy of the deconvoluted beam size strongly depends on the accuracy of the point-spread function. It is possible that the true point-spread function is more distorted than that calibrated in §4, because of the contamination by stray light, which we ignored in the calibration procedure function. If the distortion of the point-spread function is underestimated, the deconvoluted vertical beam size may be overestimated. Note that the obtained vertical beam size of 21.8 µm is a preliminary result, and the effect of contamination by stray light on the point-spread function is yet to be evaluated.

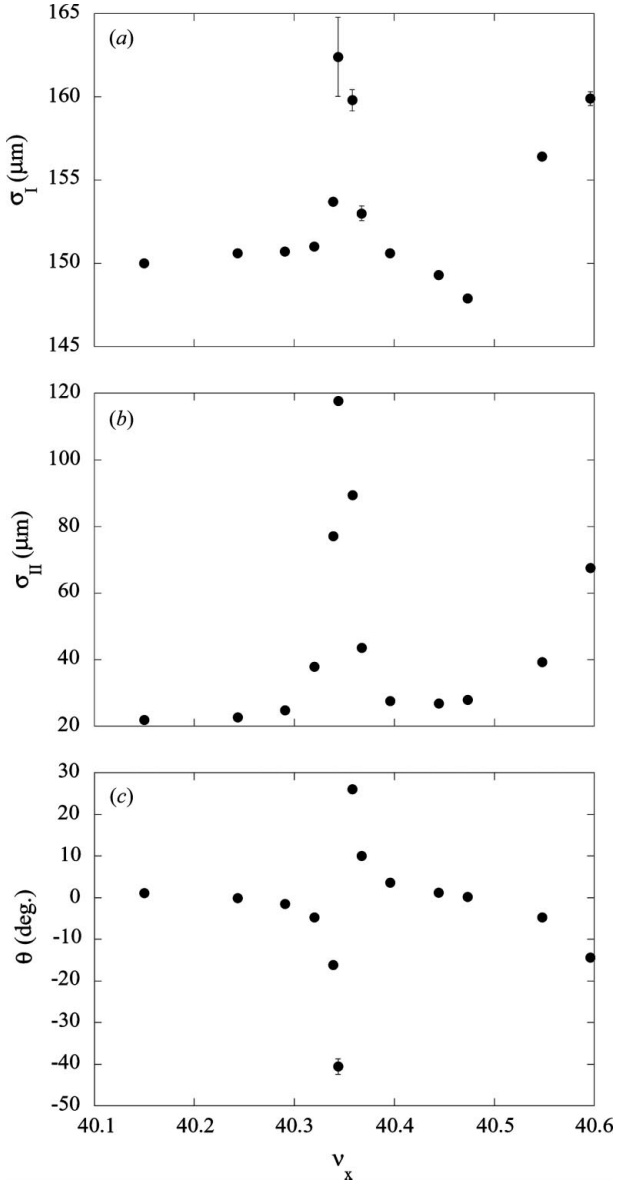

Figure 6
Results of the beam-profile measurement at the SPring-8 storage ring. (*a*), (*b*) and (*c*) show the parameters $\sigma_{\rm I}$, $\sigma_{\rm II}$ and θ, respectively. The vertical betatron tune was fixed at $\nu_y = 18.35$. The horizontal tune was varied across a differential resonance condition. The horizontal betatron tune $\nu_x = 40.35$ corresponds to the differential resonance and 40.65 corresponds to the sum resonance. The horizontal tune for users' time operation is 40.15.

5.2. Beam emittance

The electron beam emittance and the emittance-coupling ratio are expressed as

$$\varepsilon_i = \left[\sigma_i^2 - (\eta_i \sigma_{\rm E}/E)^2\right]/\beta_i, \quad i = x, y, \tag{31}$$

$$\kappa = \varepsilon_y/\varepsilon_x. \tag{32}$$

The horizontal beam emittance was found to be $\varepsilon_x = 6.57 \pm 0.33$ nm rad by using the measured horizontal beam size (150.0 ± 0.1 µm) at the working point $(\nu_x, \nu_y) = (40.15, 18.35)$. It was assumed that the betatron function at the source point and the energy spread were the designed values $\beta_x = 1.91$ m and $\sigma_E/E = 1.09 \times 10^{-3}$, respectively. The dispersion function at the source point was determined experimentally to be $\eta_x = 91.5 \pm 2.9$ mm from the measured positions of the electron beam, by changing the RF frequencies of the storage ring. The designed value of 1.46×10^{-4} for the momentum compaction factor, α, was assumed. The horizontal beam emittance of the SPring-8 storage ring was obtained to be $\varepsilon_x = 6.0 \pm 0.4$ nm rad by using a horizontal beam size in a dispersion-free straight section of the ring measured by the 'kick and scrape' method (Soutome *et al.*, 1999). The horizontal emittance obtained by this method is consistent with that obtained by the two-dimensional interferometer within the errors. The designed value of the emittance is 6.6 nm rad (Tanaka *et al.*, 2002).

The vertical beam emittance was calculated to be $\varepsilon_y = 17.7$ pm rad from the vertical beam size (21.8 µm) measured by the two-dimensional interferometer. The emittance coupling ratio, κ, in (32) was 0.27%. The vertical betatron function was assumed to be the designed value ($\beta_y = 26.9$ m) and the dispersion function at the point source was measured to be $\eta_y = -2.5 \pm 2.3$ mm. The measured vertical beam size of 21.8 µm may be overestimated by ignoring the effect of stray light, as noted in §5.1, and consequently the calculated vertical emittance may be overestimated. A vertical emittance of 4.1 pm rad was obtained from measurements of the Touschek lifetime (Tanaka *et al.*, 2000). A vertical beam size of 12.8 µm was measured by X-ray intensity interferometry at beamline BL19LXU, which had a long undulator of length 25 m as a light source (Yabashi *et al.*, 2001). A vertical emittance of 9.1 pm rad was obtained from the beam size by assuming an effective value for the betatron function of 17.97 m, which is an averaged value of the designed betatron function along the undulator. The vertical emittance obtained by two-dimensional visible light interferometry is larger than the results from the two other methods. To measure the small vertical emittance of the SPring-8 storage ring with high accuracy with the two-dimensional interferometer, it is necessary to avoid stray light by replacing the narrow upstream vacuum duct.

6. Discussion

We have developed a new two-dimensional visible synchrotron light interferometer to measure simultaneously the horizontal and vertical sizes and the tilt angle of an electron beam. The point-spread function of an interferometer installed at the SPring-8 storage ring was determined by an experimental method.

The interferometer at the SPring-8 storage ring does not have sufficient resolution for the measurement of a small vertical beam size, because the aperture of the upstream vacuum duct limits the available vertical separation of the apertures of the diffracting mask. The narrow vacuum duct also causes a problem with stray light. The measured vertical beam size of 21.8 μm is preliminary, in the sense that it is subject to contamination by stray light. To measure the small vertical beam size of the SPring-8 storage ring accurately, it will be necessary to replace the narrow duct with a wider one, which does not obstruct the synchrotron radiation. The resolution can be further improved by employing light of shorter wavelength than visible light. For example, assuming ultraviolet light with a wavelength of 220 nm and a vertical angular separation of the apertures of 3 mrad, we could achieve a resolution of 13 μm for the vertical size measurement. The separation in this case is limited by the finite extent of the synchrotron radiation.

We observed the transverse beam profile of the SPring-8 storage ring with the two-dimensional interferometer at various working points. Although the resolution for vertical size measurement was not sufficient, beam-size broadening and changes in the tilt angles near the differential and the sum resonance conditions were clearly observed. The two-dimensional profiling ability of the new interferometer has been successfully demonstrated. Two-dimensional interferometers will be useful tools for beam-profile measurements of electron storage rings, since these interferometers have approximately a two times better resolution than imaging methods.

APPENDIX *A*
Spherical-wave approximation of synchrotron radiation from a bending-magnet source

Synchrotron radiation from an electron moving in the magnetic field of a bending magnet is not a spherical wave in a strict sense. The phase of light on a diffracting mask of a two-dimensional interferometer is given by (Takayama & Kamada, 1999)

$$\Phi(x_s, y_s; x_e, y_e; x'_e, y'_e) = (2\pi/\lambda)\{L_0 + [(x_s - x_e)^2 + (y_s - y_e)^2]/(2L_0) + h(x_s, y_s; x_e, y_e; x'_e, y'_e)\}, \quad (33)$$

where

$$h(x_s, y_s; x_e, y_e; x'_e, y'_e) = \rho_0 (2L_0)^{-1} (x_s - x_e - L_0 x'_e) \times \{\gamma_0^{-2} + [(x_s - x_e - L_0 x'_e)^2 + 3(y_s - y_e - L_0 y'_e)^2]/3L_0^2\} + \cdots, \quad (34)$$

and ρ_0 is the bending radius. The parameter γ_0 denotes the Lorentz factor. If the conditions

$$\rho_0 \simeq L_0, \quad (35)$$

$$\gamma_0^2 \gg 1, \quad (36)$$

$$\sigma'_x \ll \eta_{12} \ll 1, \quad (37)$$

$$\sigma'_y \ll \eta_{14} \ll 1, \quad (38)$$

are satisfied, the third term of (33) is negligible compared with the second term, and the phase of the radiation can be approximated by that of a spherical wave. The parameters σ'_i ($i = x, y$), η_{12} and η_{14} are the angular divergence (1σ) of the electron beam, and the horizontal and vertical angular separations between the four apertures of the diffracting mask, respectively.

The conditions required to apply the spherical wave approximation to the amplitude distribution are as follows. The full width of the vertical angular divergence of the synchrotron radiation has to be sufficiently larger than the width of the vertical angular divergence of the electron beam at the source point, namely,

$$(12\lambda/\pi\rho_0)^{1/3} \gg 4\sigma'_y. \quad (39)$$

The light intensity on each aperture of the diffracting mask has to be as uniform as possible. If we assume that the vertical distribution of the synchrotron radiation is Gaussian, the condition

$$(4d\eta_{14}/L_0)(\pi\rho_0/12\lambda)^{2/3}\exp[-2\eta_{14}^2(\pi\rho_0/12\lambda)^{2/3}] \ll 1 \quad (40)$$

is derived.

The parameters of the interferometer installed at the SPring-8 storage ring are $\rho_0 = 39.27$ m, $L_0 = 19.64$ m, $\eta_{12} = 0.662$ mrad, $\eta_{14} = 1.53$ mrad, $\gamma_0 = 15656$, $\sigma'_x = 100$ μrad, $\sigma'_y = 0.5$ μrad and $\lambda = 443.48$ nm. Since conditions (35)–(40) are satisfied, it is considered that the light emitted at the source point closely approximates a spherical wave on the diffracting mask.

The authors wish to thank Dr N. Kumagai for continuous encouragement of this work and Dr H. Ohkuma for a critical reading of the manuscript and valuable comments. Drs H. Tanaka, M. Takao and K. Soutome assisted, from the viewpoint of beam dynamics, in controlling the storage-ring beam in the experiment. Dr M. Shoji and Mr M. Oishi helped in the installation of the interferometer.

References

Born, M. & Wolf, E. (1980). *Principles of Optics*, 6th ed., p. 508. Oxford: Pergamon.
Chubar, O. V. (1995). *Proceedings of the 1995 Particle Accelerator Conference*, 1–5 May 1995, Dallas, USA, p. 2447. Piscataway, NJ: IEEE.
Fizeau, H. (1868). *C. R. Acad. Sci. Paris*, **66**, 934.
Hoffmann, A. & Meot, F. (1982). *Nucl. Instrum. Methods Phys. Res.* **203**, 483.
Masaki, M., Takano, S., Tanaka, H., Soutome, K., Takao, M., Oishi, M., Tamura, K., Shoji, M., Sasaki, S. & Ohkuma, H. (1999). *Proceedings of the 12th Symposium on Accelerator Science and Technology*, Wako, Japan, p. 525.
Michelson, A. A. (1920). *Astrophys. J.* **51**, 257.
Mitsuhashi, T. (1997). *Proceedings of the 1997 Particle Accelerator Conference*, Vancouver, Canada, p. 776. Piscataway, NJ: IEEE.
Mitsuhashi, T. & Naito, T. (1998). *Proceedings of the 1998 European Particle Accelerator Conference*, Stockholm, Sweden, p. 1565. Bristol: IOP.
Soutome, K., Tanaka, H., Takao, M., Kumagai, K., Ohkuma, H. & Kumagai, N. (1999). SPring-8 Annual Report, p. 136. SPring-8, Hyogo, Japan.
Takayama, Y. & Kamada, S. (1999). *Phys. Rev. E*, **59**, 7128.
Tanaka, H., Kumagai, K., Kumagai, N., Masaki, M., Ohkuma, H., Soutome, K. & Takao, M. (2000). *Proceedings of the 2000 European Particle Accelerator Conference*, Vienna, Austria, p. 1575. Geneva: European Physical Society.
Tanaka, H., Soutome, K., Takao, M., Masaki, M., Ohkuma, H., Kumagai, N. & Schimizu, J. (2002). *Nucl. Instrum. Methods Phys. Res. A*, **486**, 521.
Yabashi, M., Tamasaku, K. & Ishikawa, T. (2001). *Phys. Rev. Lett.* **87**, 140801.